

New light on Dark Cosmos

Enrique Gaztañaga^{1,2}, Marc Manera¹, Tuomas Multamäki³

¹ *Institut d'Estudis Espacials de Catalunya, IEEC/CSIC, F. de Ciències, Torre C5 Par 2a, UAB, Bellaterra (08193 BARCELONA)*

² *Visiting: INAOE, Tonanzintla, P.O.Box 51, 7200 Puebla, Mexico*

³ *NORDITA, Blegdamsvej 17, DK-2100, Copenhagen, Denmark*

17 September 2018

ABSTRACT

Recent studies by a number of independent collaborations, have correlated the CMB temperatures measured by the WMAP satellite with different galaxy surveys that trace the matter distribution with light from the whole range of the electromagnetic spectrum: radio, far-infrared, optical and X-ray surveys. The new data systematically finds positive correlations, indicating a rapid slow down in the growth of structure in the universe. Individual cross-correlation measurements are of low significance, but we show that combining data at different redshifts introduces important new constraints. Contrary to what happens at low redshifts, for a fixed Ω_m , the higher the dark energy content, Ω_Λ , the lower the ISW cross-correlation amplitude. At 68% confidence level, the data finds new independent evidence of dark energy: $\Omega_\Lambda = 0.42 - 1.22$. It also confirms, to higher significance, the presence of a large dark matter component: $\Omega_m = 0.18 - 0.34$, exceeding the density of baryonic matter, but far from the critical value. Combining these new constraints with the prior of a flat universe, or the prior of an accelerating universe provides strong new evidence for a dark cosmos. Combination with supernova data yields $\Omega_\Lambda = 0.71 \pm 0.13$, $\Omega_m = 0.29 \pm 0.04$. If we also assume a flat universe, we find $\Omega_\Lambda = 0.70 \pm 0.05$ and $w = -1.02 \pm 0.17$ for a constant dark energy equation of state.

1 INTRODUCTION

In the last few years a new cosmological scenario with a significant smooth Dark Energy (DE) component has emerged. The Cosmic Concordance Model (CCM, from now on) is a spatially flat universe with baryons ($\Omega_b \sim 4\%$), cold dark matter ($\Omega_{CDM} \sim 23\%$) and a significant DE component ($\Omega_\Lambda \sim 73\%$). The model is well supported by the supernova type Ia observations (SNIA) (Riess et al. 1998; Perlmutter et al. 1999), observations on large scale structure (LSS) (Tegmark et al. 2004; Percival et al. 2001) and the cosmic microwave background experiments (CMB), in particular by the recent WMAP experiment (Bennett et al. 2003). The energy density of the universe seems dominated by the unknown DE component, presenting a formidable observational and theoretical challenge. The three key observational probes measure complementary aspects of the cosmological parameter space. The SNIA indicate that the universe is accelerating but present data is degenerate for alternative cosmological scenarios. The LSS observations constrain Ω_m but leave the DE question unanswered. Constraints from primary anisotropies in the CMB indicate that we live in a flat universe but require a prior on the value of the local Hubble rate H_0 (Blanchard 2003). Assuming that the universe is well described by a Λ CDM model, combining all these three observations gives us the cosmological CCM model.

The Integrated Sachs Wolfe effect, ISW, (Sachs & Wolfe 1967) is a direct probe for the (linear) rate of structure formation in the universe. Secondary anisotropies in the CMB appear because of the net gravitational redshifts affecting CMB photons that travel through an evolving gravitational potential Φ . These secondary temperature anisotropies are therefore correlated with local, evolving, structures on large scales. The correlation is negative when structures grow, as increasing potential leaves a cold spot in the CMB sky, and positive otherwise. In a flat universe without DE (Einstein-deSitter, or EdS, model) this cross-correlation is expected to be zero because the gravitational potential remains constant, despite the linear growth of the matter fluctuations.

The rate of structure formation in the universe can also be measured by galaxy peculiar velocities or galaxy redshift distortions, on very large scales through the so-call β parameter determination (Peacock et al. 2001; Pope et al. 2004). The ISW effect provides an independent and complementary probe of the same effect. Independent, because it uses temperature anisotropies instead of the velocity field, and complementary, because of the different assumptions and systematics that relate measurements with theory. Despite recent advances in the size of galaxy redshift surveys such as SDSS and 2dFGRS, the spectrum of matter fluctuations $P(k) \propto \langle \delta(k)^2 \rangle$ is quite difficult to measure directly over very large scales (Tegmark et al. 2004; Percival et al. 2001;

Gaztañaga & Baugh 1998). Part of the problem is that matter correlations fall quickly to zero on scales larger than 30 Mpc/h ($k < 0.1$ h/Mpc). In contrast, fluctuations in the gravitational potential go as $\Phi(k) \propto \delta(k)/k^2$ and therefore extend over larger distances, which makes the signal more detectable (see also comments to Fig. 4). The ISW cross-correlation traces the gravitational potential, Φ , and thus provides a new window to study the largest structures, extending over several degrees in the sky or tens of Mpc/h at the survey depth.

2 GROWTH OF DENSITY PERTURBATIONS

Gravitational evolution of matter fluctuations, $\delta = \rho/\bar{\rho} - 1$, is dependent on the cosmological model via the evolution of the scale factor $a = a(t)$. Compared to a static background, a rapidly expanding background will slow down the collapse of an over dense region. In the linear regime, a small initial perturbation δ_0 grows according to the growth factor $D(t)$:

$$\delta(t) = D(t) \delta_0 \quad (1)$$

which, under quite generic assumptions, eg (Gaztañaga & Lobo 2001; Multamäki, Gaztañaga & Manera 2003; Lue & Starkman 2004), follows a simple harmonic equation:

$$\frac{d^2 D}{d\eta^2} + \left(2 + \frac{\dot{H}}{H^2}\right) \frac{dD}{d\eta} + 3c_1 D = 0, \quad (2)$$

where $\eta = \ln(a)$ is the conformal time and $H = H(\bar{\rho}) \equiv \dot{a}/a$ is the background Hubble rate (\dot{a} and \dot{H} are proper time derivatives). For a flat cosmological model with a generic dark energy equation of state

$$p = w(z)\rho \quad (3)$$

we then have:

$$H^2 = \left(\frac{\dot{a}}{a}\right)^2 = H_0^2 \left[\Omega_m (1+z)^3 + \Omega_\Lambda e^3 \int_0^z \frac{dz'}{1+z'} (1+w(z')) \right] \quad (4)$$

where Ω_Λ and Ω_m are the dark energy and dark matter densities today in units of the critical density $\rho_c \equiv 3H^2/(8\pi G)$. And c_1 is given by:

$$c_1 = -\frac{1}{2} \frac{H_0^2 \Omega_m (1+z)^3}{H^2(z)} \quad (5)$$

In this paper we study two cases. A generic (not necessarily flat) Λ CDM model where DE density is constant over the evolution of the universe ($w = -1$); and a flat Λ CDM model with a constant equation of state parameter. For those models we have

$$c_1 = -(1/2) \Omega_m / (\Omega_m + \Omega_\Lambda a^3) \quad (6)$$

One may choose to compare the results to the EdS model: $\Omega_\Lambda = 0$, $\Omega_m = 1$, in which case the solution to Eq. (2) is $D \propto a$. This means that δ grows linearly with the scale factor, $\delta \propto a$, while the corresponding gravitational potential fluctuation, $\Phi \sim \delta/a$, remains constant as the universe expands. For non EdS models Φ would change during the expansion of the universe which would turn into a galaxy-CMB temperature cross-correlation signal.

2.1 The ISW effect

ISW temperature anisotropies are given by (Sachs & Wolfe 1967):

$$\Delta_T^{ISW}(\hat{n}) \equiv \frac{T(\hat{n}) - T_0}{T_0} = -2 \int dz \frac{d\Phi}{dz}(\hat{n}, z) \quad (7)$$

where Φ is the Newtonian gravitational potential at redshift z . One way to detect the ISW effect is to cross-correlate temperature fluctuations with galaxy density fluctuations projected in the sky (Crittenden & Turok 1996). On large linear scales and small angular separations, the cross-correlation $w_{TG}^{ISW}(\theta) = \langle \Delta_T^{ISW}(\hat{n}_1) \delta_G(\hat{n}_2) \rangle$ is (Fosalba & Gaztañaga 2004):

$$\begin{aligned} w_{TG}^{ISW}(\theta) &= \frac{1}{2\pi} \int \frac{dk}{k} P(k) g(k\theta) \\ g(k\theta) &= \int dz W_{ISW}(z) W_G(z) \frac{H(z)}{c} J_0(k r_A \theta) \\ W_{ISW}(z) &= 3\Omega_m (H_0/c)^2 \frac{d[D(z)/a]}{dz} \\ W_G(z) &= b(z) \phi_G(z) D(z), \end{aligned} \quad (8)$$

where J_0 is the zero order Bessel function, ϕ_G is the survey galaxy selection function along the line of sight z and $r_A = r_A(z)$ the comoving transverse distance. The power spectrum is $P(k) = A k^{n_s} T^2(k)$, where $n_s \simeq 1^1$ and $T(k)$ is the Λ CDM transfer function, which we evaluate using the fitting formulae of Einseintein & Hu 1998. We make the common assumption that galaxy and matter fluctuations are related through the linear bias factor, $\delta_G(\hat{n}, z) = b(z)\delta_m(\hat{n}, z)$.

For the Λ CDM case the ISW effect is non-zero, and the kernel W_{ISW} can be well approximated by $W_{ISW}(z) = -3\Omega_m (H_0/c)^2 D(z)(f-1)$, where f is the relative growth factor, $f \simeq \Omega_m(z)^{6/11}$. W_{ISW} decreases as a function of increasing redshift and goes to zero both for $\Omega_m \rightarrow 0$ and for $\Omega_m \rightarrow 1$. At low redshifts, the ISW effect is larger for larger values of Ω_m , but the redshift evolution depends on the curvature (ie how quickly the H and D evolve to the EdS case). This is illustrated in Fig.1 which shows how W_{ISW} depends on z for different values of Ω_Λ and Ω_m . At high redshifts, the lower the value of Ω_Λ (for a fixed Ω_m) the larger the ISW amplitude.

In Figures 2 and 3 we also shown for a given flat cosmology model the dependence of the W_{ISW} on redshift and on the equation of state parameter w . For a given redshift and Ω_m there exists a maximum of W_{ISW} around $w = -0.5$. This maximum would translate into a maximum in the cross-correlation signal w_{TG} . If data turns out to be greater than this maximum this would clearly disfavor models with constant equation of state.

¹ Throughout the paper we made the assumption of scale invariant primordial fluctuations ($n_s \simeq 1$). For other possibilities see, eg, (Barriga et al 2001).

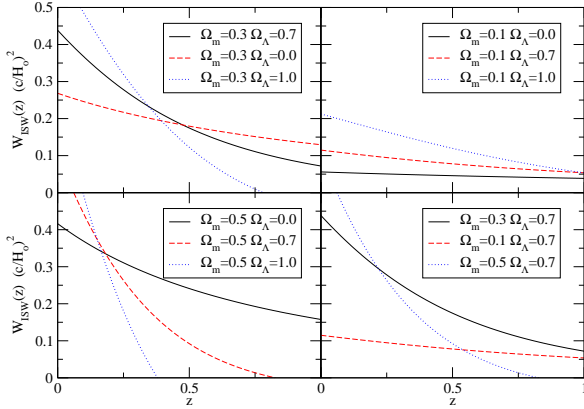


Figure 1. Redshift dependence of $W_{ISW}(z)$ in Eq.[8] for different values of Ω_m and Ω_Λ . Bottom left, top right and top left panels shows a fixed $\Omega_m = 0.5$, $\Omega_m = 0.3$ and $\Omega_m = 0.1$ respectively. In all cases: $\Omega_\Lambda = 0.0$ (dotted blue line), $\Omega_\Lambda = 0.7$ (continuous black line) and $\Omega_\Lambda = 1.0$ (dashed red line). Bottom right panel shows a fixed $\Omega_\Lambda = 0.7$ and $\Omega_m = 0.3$ (continuous black line), $\Omega_m = 0.5$ (dotted blue line) and $\Omega_\Lambda = 0.1$ (dashed red line).

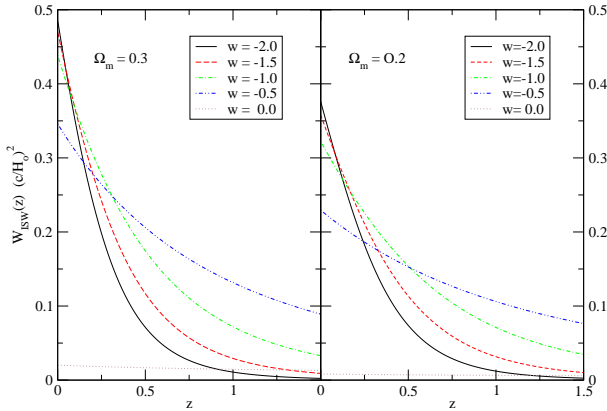


Figure 2. Redshift dependence of W_{ISW} in eq [8] for flat models with constant equation of state. Right panel shows a fixed $\Omega_m = 0.2$ and left panel $\Omega_m = 0.3$. In both cases $w = -2$ (black continuous line), $w = -1.5$ (red dashed line), $w = -1$ (green dot-dashed line), $w = -0.5$ (blue double-dot-dashed line), and $w = 0$ (brown dotted line)

2.2 Bias Self-calibration

Linear bias is used to study how well light traces the underlying statistics of linear matter fluctuations. On these very large scales, fluctuations δ are small and linear theory works very well both for biasing and gravity. We remove the effects of biasing in our parameter estimation by comparing the observed galaxy-galaxy correlation w_{GG} , in the very same samples used for the cross-correlation, to the matter-

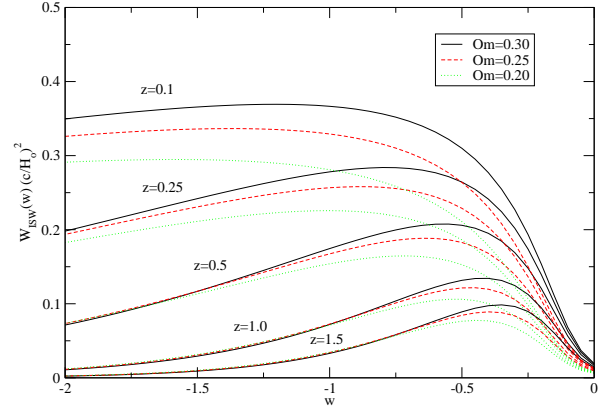


Figure 3. Dependence of W_{ISW} on the equation of state parameter w for flat models at different redshifts and values of Ω_m . $\Omega = 0.3$ (back continuous lines), $\Omega_m = 0.25$ (red dashed lines), $\Omega_m = 0.2$ (green dotted lines). Redshifts are 0.1, 0.25, 0.5, 1.0, 1.5 from top to bottom.

matter correlation w_{mm} predicted by each model (Fosalba, Gaztañaga & Castander 2003). The effects of bias are also redshift dependent, but given a galaxy selection function $\phi_G(z)$, picked at $z = \bar{z}$, we approximate the bias with a constant $b = b(\bar{z})$ for that particular survey. We then have: $w_{TG} = b(\bar{z})w_{Tm}$ and $w_{GG} = b^2(\bar{z})w_{mm}$, so that an effective linear bias b can be estimated as the square root of the ratio of galaxy-galaxy and matter-matter correlation functions:

$$b = \sqrt{\frac{w_{GG}}{w_{mm}}}. \quad (9)$$

Such prescription has been shown to work well in a variety of galaxy models (eg see (Berlind, Naratanan & Weinberg 2001)). The values of w_{mm} can be computed similar to (8) by

$$w_{mm}(\theta) = \frac{1}{2\pi} \int dk k P(k) g(k\theta) \quad (10)$$

$$g(k\theta) = \int dz W_m^2(z) \frac{H(z)}{c} J_0(k r_A \theta)$$

$$W_m(z) = \phi_G(z) D(z),$$

where the only difference between W_m and W_G is the bias factor $b(z)$ in Eq.[8]. Note how the estimation of b in Eq.[9] depends on the normalization of the power spectrum in w_{mm} . We choose to normalize each model by fixing σ_8 . To make our results independent of this normalization we will marginalize over σ_8 and h . Taking flat priors and ranges $\sigma_8 = 0.8 - 1.0$ and $h = 0.72 - 0.77$. We compare the predictions with the observational data w_{TG} normalized to the CCM model bias, ie w_{TG}/b , where b is estimated from Eq. (9) using w_{mm} in the CCM model. Consequently, for other models, we will need to renormalize each of the theoretical predictions to the CCM model bias using a “relative bias”:

$w_{TG}^{mod}/b = b_r w_{tm}^{mod}$, where $b_r^2 = w_{mm}/w_{mm}^{mod}$ is the ratio of the concordance model prediction to the one in the corresponding model. We choose to estimate this relative bias at $R = 8$ Mpc/h, but the actual number has little effect in our final conclusions.

3 OBSERVATIONAL DATA

Recent analysis by independent collaborations, have cross-correlated the CMB anisotropies measured by WMAP with different galaxy surveys. The median galaxy redshifts expand over a decade (ie $0.1 < \bar{z} < 1.0$) and trace the matter distribution with light from the whole range of the electromagnetic spectrum: radio, far-infrared, optical and X-ray surveys (see Table 1). The cross-correlation and error estimation techniques used are also quite different but they yield comparable results over the scales of interest. Compare for example the Montecarlo errors to jackknife errors in Fig.3 in Fosalba & Gaztañaga (2004). In our compilation of the different data sets, we average the results on fixed angular scales around $\theta = 6^\circ$. This corresponds to proper distances of $\simeq 25$ Mpc/h at $\bar{z} \simeq 0.1$ and $\simeq 100$ Mpc/h at $\bar{z} \simeq 1.0$ in the CCM model and avoids possible contamination from the small scale SZ and lensing effects, eg see Fig. 3 in Fosalba, Gaztañaga & Castander (2003).

Radio galaxies from NVSS (Condon et al 1998) and hard X-ray background observed by HEAO-1 (Boldt 1987), have been cross-correlated with WMAP data (Boughn & Crittenden 2004a; Boughn & Crittenden 2004b), to find a signal of 1.13 ± 0.35 times the CCM model prediction at $z \sim 0.9$. The different biases for X-rays, $b^2 = 1.12$, (Boughn & Crittenden 2003) and for radio galaxies, $b = 1.3 - 1.7$, (Boughn & Crittenden 2002) have been taken into account. A compatible signal has also been found with the NVSS data by the WMAP team (Nolta et al. 2004).

The cross correlation of WMAP with galaxies ($17 < b_J < 20$) in the APM Galaxy Survey (Maddox et al. 1990) (covering about 20% of the South Galactic Cap, SGC) was found to be $w_{TG} = 0.35 \pm 0.13 \mu K$ at scales $\theta = 4 - 10^\circ$ with $b \simeq 1$ (Fosalba & Gaztañaga 2004). The cross-correlation of WMAP with the SDSS DR1 (Tegmark et al. 2004) (covering about 10% of the North Galactic Cap, NGC) have been done for several subsamples (Fosalba, Gaztañaga & Castander 2003). The first sample ($\bar{z} \sim 0.3$) contains ~ 5 million objects classified as galaxies in SDSS (with $r < 21$ and low associated error). For this sample, which has $b \simeq 1$, $w_{TG} = 0.26 \pm 0.13 \mu K$ at scales $\theta = 4 - 10^\circ$. The high redshift sample ($z \sim 0.5$) has $w_{TG} = 0.53 \pm 0.21 \mu K$ and $b^2 \simeq 6$. The SDSS data has also been cross-correlated with WMAP by the SDSS team (Scranton et al. 2003) using nearly 25 million galaxies in four redshift samples. Their results are similar with those obtained earlier by Fosalba, Gaztañaga & Castander (2003) but no bias from galaxy-galaxy auto correlation function is given. The infrared 2MASS Galaxy Survey (Jarret et al. 2000), with $z \sim 0.1$, show a WMAP cross-correlation of 1.53 ± 0.61 times the CCM prediction, with a bias of $b = 1.18$ (Afshordi, Loh & Strauss 2004).

We have selected independent measurements for which the bias CCM b (from w_{GG}) is known, so that we can applied

\bar{z}	w_{TG}/b	b	catalog, Band
0.1	0.70 ± 0.32	1.1	2MASS, infrared ($2\mu m$)
0.15	0.35 ± 0.17	1.0	APM, optical (b_j)
0.3	0.26 ± 0.14	1.0	SDSS, optical (r)
0.5	0.216 ± 0.096	2.4	SDSS high-z, optical (r +colors)
0.9	0.043 ± 0.015	1-2	NVSS+HEAO, Radio & X-rays

Table 1. Observed cross correlation w_{TG}/b (averaged for $\theta \simeq 4 - 10^\circ$.) of WMAP anisotropies with different catalogs. Errors in w_{TG}/b includes 20% uncertainty in b . Errors in the median redshift \bar{z} are about 10% .

the bias “self-calibration” proposed in section §2.2. The data is summarized in Table 1 and displayed in Fig.1. In the results below we also include a 10% uncertainty in the median redshift. We chose the values of NVSS+HEAO-1 quoted by (Boughn & Crittenden 2004b) as representative of both the Nolta et al. (2004) and Boughn & Crittenden (2004a) analysis. For the SDSS, we chose the values in Fosalba & Gaztañaga (2004) where the CCM bias b is estimated using Eq.(9). Note how the selected samples are complementary. The samples which have large sky overlap (eg 2MASS and NVSS+HEAO-1) have negligible redshift overlap. When the redshift overlap is significant (ie in 2MASS-APM or SDSS-NVSS could be up to 20%) the sky overlap is small (less than 10%). Consequently, the different samples in Table 1 have less than 1% volume in common. This is negligible, given that individual sampling errors (which are proportional to volume) are of the order of 30%.

The most significant detection in Table 1 seems to be the one quoted by Boughn & Crittenden (2004b) for the NVSS+HEAO-1 samples. Given the systematic uncertainties involved in the bias and selection function of both of these samples, we have checked that our results do not changed much (less than 20% in the area of the contours in Fig.3) when we double the quoted errorbar. Doubling this errorbar corresponds to an additional 50% systematic uncertainty in the value b or to a 40% uncertainty in the median redshift of the samples.

The observational data not included in Table 1 is in good agreement with the values in the table, but is excluded to avoid redundancy. The agreement of the redundant data provides further confirmation and indicates that errors are dominated by sampling variance rather than by the methodology or the systematics.

4 RESULTS

Fig.4 compares the w_{TG} observations with predictions for a fixed value of $\Omega_m = 0.3$ and three different values of Ω_Λ . We can see how the shape of the prediction depends on the amount of dark energy. Even though W_{ISW} at $z = 0$ depends only weakly on Ω_Λ , the evolution with redshift depends more strongly on Ω_Λ . For a fixed Ω_m , models with larger values of Ω_Λ evolve more rapidly with redshift to the EdS case, where the ISW effect vanishes. Thus, contrary to what happens at $z = 0$, the lower the value of Ω_Λ (for a fixed Ω_m) the larger the ISW amplitude at high redshifts (see also Fig.1).

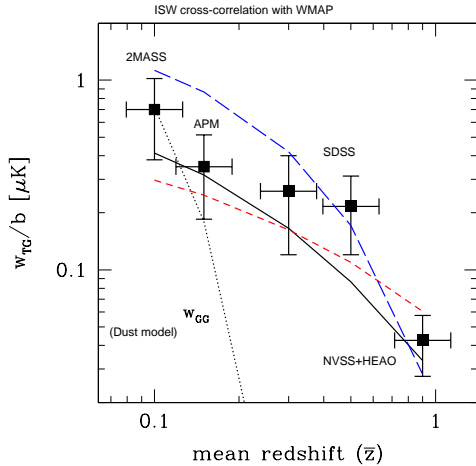


Figure 4. Symbols with error bars correspond to the different measurements w_{TG}/b in Table 1. As an illustration of the shape, the continuous, short-dashed and long-dashed lines show the concordance ($\Omega_m = 0.3, \Omega_\Lambda = 0.7$), opened ($\Omega_m = 0.3, \Omega_\Lambda = 0.0$) and closed ($\Omega_m = 0.3, \Omega_\Lambda = 1.1$) model predictions (at $\theta = 6^\circ$). The dotted line corresponds to the galaxy-galaxy prediction (and also the dust contamination model). All lines have arbitrary normalization.

To test model predictions with the data, we use a standard χ^2 -test, $\chi^2 = \sum_i (O_i - T_i)^2 / \sigma_i^2$, where O_i and σ_i correspond to the different measurements and errors and T_i correspond to the model. The label i runs for $i = 1$ to $i = 5$ marking the different data points (column 1 in Table 1) as we move in redshift. In order to take into account the error in the median redshift we take:

$$\sigma_i^2 = \sigma_w^2 + \left(\frac{d(w_{tg}/b)}{dz} \right)^2 \sigma_z^2 \quad (11)$$

where σ_z and σ_w are the errors in the w_{TG}/b and \bar{z} respectively (see Table 1). We use the relative χ^2 values, $\chi^2 - \chi_{min}^2$, to define confidence levels in parameter estimation. Top panel of Fig.5 shows the resulting confidence contours. Taking $T_i = 0$ we evaluate the significance of the combined ISW detection. We find that this null hypothesis is rejected with a very high probability: $P \simeq 99.997\%$ (from $P_{\nu=4}(\chi^2 > 26) \simeq 3 \times 10^{-5}$). We next compute the expected ISW effect and compare it with the observational data within the Λ CDM family of models, where Ω_m , Ω_Λ and h ² are free parameters (we fix the baryonic content $\Omega_b \simeq 0.05$ and the primordial spectral index $n_s \simeq 1$). We choose to normalize each model by fixing σ_8 . To make our results independent of this normalization we will marginalize σ_8 over the range $\sigma_8 = 0.8 - 1.0$ (flat prior used). As we compare w_{GT} normalized to the CCM model bias, we need to compute the relative bias for other Λ CDM models (see section §2.2). We choose to estimate this at $R = 8 \text{ Mpc}/h$, but the actual number has little effect in the conclusions. We have also marginalized over h in a flat prior range $h = 0.72 - 0.77$. Our results are not very sensitive to the

² We use $H_0 \equiv 100 h \text{ km/s/Mpc}$.

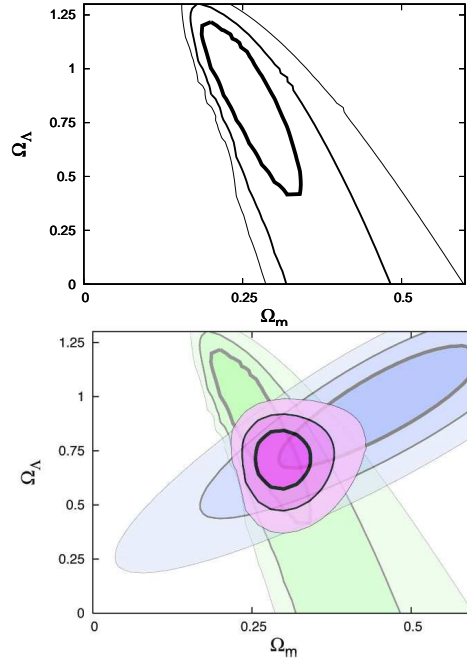


Figure 5. One, two and three sigma confidence contours in the $(\Omega_m, \Omega_\Lambda)$ plane (marginalized over h) for the Λ CDM model. Top: constraints from only ISW. Bottom: constraints from SNIa (blue) and ISW (green) along with the combined contours (purple).

ranges used for σ_8 and h : increasing these ranges by a factor of two change our contours in less than 20 %.

The best fit using only ISW data corresponds to $\Omega_m \simeq 0.26 \pm 0.08$, $\Omega_\Lambda \simeq 0.82 \pm 0.40$, in good agreement with other cosmological probes mentioned above. Bottom panel of Fig. refcombinedconts we show the confidence contours for a Λ CDM model along with the constraints from recent SNIa (Barris et al. 2004) observations. From the figure it is clear how the ISW effects gives new complementary information about the cosmological parameters. The EdS model is ruled out to high significance. The confidence contours are almost perpendicular to the SNIa contours, allowing to constrain the parameter space of the model well with just these two observations. Combination of ISW with supernova data yields $\Omega_\Lambda = 0.71 \pm 0.13$ and $\Omega_m = 0.29 \pm 0.04$.

4.1 Uncertainties in the selection function

We explore here how robust are our results to the uncertainties in the galaxy selection function. We take a generic parametric form of the type:

$$\phi(z)dz = \frac{1}{\Gamma(\frac{m+1}{\beta})} \beta \frac{z^m}{z_0^{m+1}} e\left(-\frac{z}{z_0}\right)^\beta dz \quad (12)$$

so that it is normalized to unity. Parameters β and m control the shape of the function and are treat as fix parameters; z_0 is being changed accordingly to the median redshift \bar{z} we want for the selection function. When computing our results we use $\beta = 1.5$ and $m = 2$, in which case $\bar{z} = 1.41z_0$.

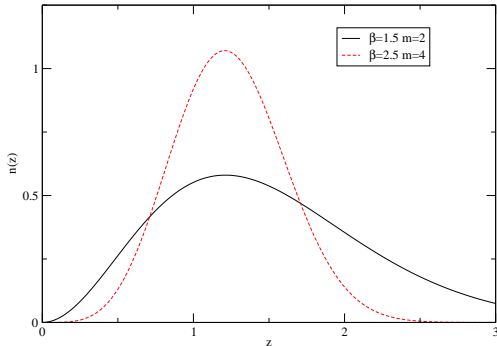


Figure 6. Two different selection functions with the same median redshift $\bar{z} = 1.41$. Both have the generic form given by the equation [12]. The black continuous line corresponds to $\beta = 1.5$ and $m = 2$ while the red dashed line is for $\beta = 2.5, m = 4$

In order to clarify the role of the selection function shape we recalculate our results with a much more peaked selection function. This second selection function has $\beta = 2.5$ and $m = 4$ and it is plotted together with the fiducial one in Figure 6. Both cases have the same median redshift $\bar{z} = 1.41$. Top panel of Fig.7 shows the contours in the $(\Omega_m, \Omega_\Lambda)$ plane for the more peaked selection function (with $\beta = 2.5$ and $m = 4$). The contours are similar to the fiducial model (ie compare to Fig. 5) but favoring slightly lower values for Ω_Λ and Ω_m .

Besides the uncertainty on the shape of the selection function there is also uncertainty in the median redshift. We have checked what happens if this uncertainty is not taken into account. We just set the redshift errors $\sigma_z = 0$ in Eq.[11]. Contours for the $(\Omega_m, \Omega_\Lambda)$ plane are plotted in the bottom panel of figure 7, which are also to compare with figure 5. There is hardly any difference because the theoretical values of w_{TG} change very little within the median redshift error range.

4.2 Equation of state

The ISW effect can also be used to constrain the dark energy equation of state parameter. In this case, as suggested by the CCM, we assumed a flat universe. We focus on a constant w parameter and maintain the same flat priors for h and σ_8 ($0.72 < h < 0.77$ $0.8 < \sigma_8 < 1.0$). Top panel of Figure 8 shows the one, two and three sigma contours for the (Ω_m, w) plane using only the ISW data. Joint contours with the SNIa data are shown in the bottom panel of Figure 8. Both datasets are also complementary for the w determination. The SNIa data is from (Barris et al. 2004).

Making a joint ISW+SNIa analysis with the flat prior reduces notably the allowed space for the parameters to $w = -1.02 \pm 0.17$ and $\Omega_\Lambda = 0.70 \pm 0.05$. The contours are comparable with other analysis in literature (Sandvik et al 2004) which combines SNIa with WMAP and SDSS data.

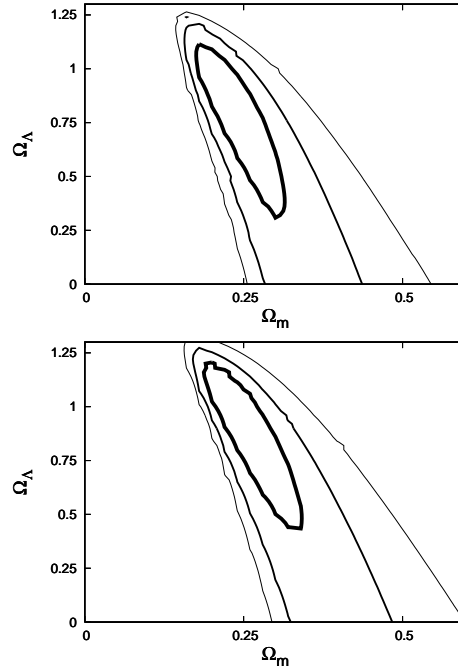


Figure 7. One, two and three sigma confidence contours in the $(\Omega_m, \Omega_\Lambda)$ plane for the Λ CDM model. Top panel: contours using a more peaked selection function ($\beta = 2.5, m = 4$) but with the same mean redshift as the fiducial case (ie compare to Fig.5). Bottom panel: contours when errors in the median redshift of the selection functions are neglected.

The results we found are still in full agreement to the CCM with $\Omega_\Lambda \simeq 0.7$ and $w = -1$.

4.3 Possible Contaminants

The constraining power of the new ISW data comes from the simultaneous fitting of data at different redshifts, that is from the shape information in Fig. 4. Because of the uncertainties in the relative normalization due to a relative bias, any given point alone does not constrain well the cosmological parameters. But the combination of the data gives us a new powerful tool for cosmological parameter estimation.

The shape of the curve as a function of redshift also provides an important test for systematics. CMB and galaxy maps are both masked and corrected from galactic absorption/extinction, but any residual contamination could produce a cross-correlation signal. Emission and absorption by our own galaxy produce patchy hot spots in the CMB maps and negative density fluctuations in the galaxy distribution (because of extinction). In principle, this should therefore result in a negative cross-correlation, but overcorrecting for the effects of galactic absorption could also result in a positive signal. This possibility has been tested for each of the samples, by comparing the cross-correlation to WMAP maps at different frequencies. Most analysis use the WMAP Kp0 mask, which excludes about 30% of sky on the basis of galactic or extra-galactic (eg radio sources) contamination. In all cases the contamination seems smaller than the errors

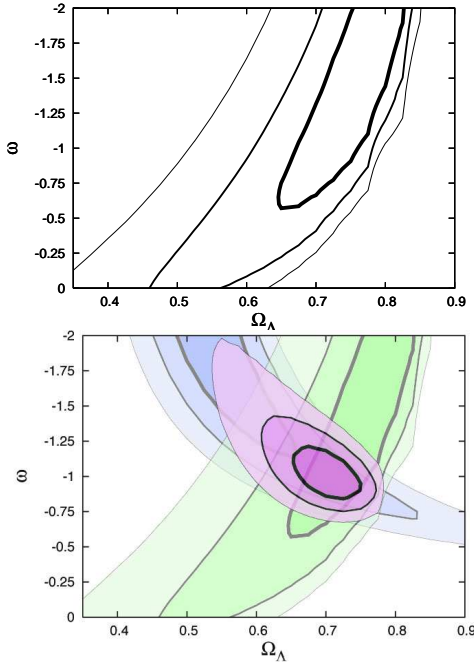


Figure 8. One, two and three sigma confidence contours in the (Ω_Λ, w) plane (marginalized over h and σ_8). Top: constraints only from ISW. Bottom: constraints from SNIa (blue) and ISW (green) along with the combination (purple).

(eg see Fig. 2 in Fosalba & Gaztañaga (2004)). Moreover, one does not expect this effect to have any redshift dependence, contrary to the measurements in Fig. 4.

Cold dust in distant galaxies, will also produce patchy hot spots in the CMB maps and positive density fluctuations in the galaxy distribution (could also be negative because of internal extinction). The resulting cross-correlation should trace the galaxy-galaxy auto correlation function, w_{GG} , and should therefore have a very different redshift dependence to the ISW effect. The dotted line in Fig. 4 shows the predicted shape dependence for w_{GG} contamination with arbitrary normalization. The shape is clearly incompatible with the actual cross-correlation measurements. It is also worth noting how w_{GG} goes quickly to zero at $\bar{z} \simeq 0.2$, while the ISW cross-correlation remains positive. This is due to the fact that at these corresponding large scales, $\gtrsim 40$ Mpc/h, matter-matter correlations w_{mm} effectively decays to zero, while w_{TG} , which traces the gravitational potential, has a less rapid decay with distance.

5 CONCLUSION

The cross-correlation of CMB anisotropies with very different galaxy surveys provides consistent detections. Their combination follows the CCM predictions with a probability of only $\simeq 3 \times 10^{-5}$ for being a false detection. This provides new and independent evidence for dark energy and dark matter, ruling out the EdS model to a high significance (for any value of H_0). Combination with SNIA data results in

strong constraints to $\Omega_\Lambda = 0.71 \pm 0.13$ and $\Omega_m = 0.29 \pm 0.04$. This is in good agreement with the flat universe $\Omega_m + \Omega_\Lambda \simeq 1$ found independently by CMB data (Bennett et al. 2003; Tegmark et al. 2004). If we assume a flat universe, we find $\Omega_\Lambda = 0.70 \pm 0.05$ and $w = -1.02 \pm 0.17$ for a constant dark energy equation of state. The data shows, for the first time, statistical evidence of a recent slow down in the growth of structure formation on linear scales, just as expected in a flat accelerated universe. The new ISW constraints rely in a totally different physical effect that previous cosmological constraints, providing new light on a dark cosmos.

Note added in proof: After this paper was originally submitted to astro-ph (astro-ph/0407022) a related analysis using our data compilation have been published by Corasaniti, Giannantonio and Melchiorri (astro-ph/0504115).

ACKNOWLEDGEMENTS

Acknowledgements: We acknowledged support from the Spanish Ministerio de Ciencia i Tecnologia, project AYA2002-00850 with EC-FEDER funding, and from the Catalan Departament d'Universitats, Recerca i Societat de la Informaci.

REFERENCES

- Afshordi, N., Loh, Y., Strauss, M. A., 2004, Phys. Rev. D 69, 083524
 Afshordi, N., 2004 astro-ph/0401166.
 Barriga, J., Gaztañaga, E., Santos, M. G., Sarkar, S., 2001, MNRAS 324, 977
 Barris, B. J. et al., 2004, ApJ 602, 571.
 Bennett C.L. et al., 2003, ApJ Suppl., 148,1
 Berlind, A., Narayanan, V., Weinberg, D., 2001, ApJ 549, 688
 Blanchard, A., Douspis, M., Rowan-Robinson, M., Sarkar, S., 2003, A&A, 412, 35.
 Boldt, E., 1987, Phys. Rep. 146, 215.
 Boughn, S., Crittenden, R. 2004, Nature 427, 45
 Boughn, S., Crittenden, R. 2004, astro-ph/0404470
 Boughn, S., Crittenden, R. 2003, astro-ph/0305001
 Boughn, S., Crittenden, R. 2002, Phys. Rev. Lett. 88, 021302
 Condon J. J. et al., 1998, AJ 115, 1693
 Crittenden, R. G. Turok, N., 1996, Phys. Rev. Lett. 76, 575.
 D.J. Einselein & W. Hu, 1998, Astrophys. J. 496, 605
 Fosalba, P. Gaztañaga, E., 2004, MNRAS 350, 37
 Fosalba, P. Gaztañaga, E., Castander, F.J., 2003, ApJ 597, L89
 Gaztañaga, E. & Baugh, C. M., 1998, MNRAS, 294, 229
 Gaztañaga, E., & Lobo, J. A., 2001, ApJ 548, 47
 Jarret, T. H., et al., 2000, AJ 119, 2498
 Lue, A., Scoccimarro, R., Starkman, G., 2004, Phys. Rev. D, 69, 044005
 Maddox, S. J., Efstathiou, G., Sutherland, W. J., Loveday, J., 1990, MNRAS 242, 43P
 Multamäki, T., Gaztañaga, R., Manera, M., 2003, MNRAS 334, 761
 Nolta, M. R. et al. 2004, ApJ 608, 10
 Peacock, J. A. et al., 2001, Nature, 410, 169
 Percival W.J. et al., 2001, MNRAS, 327, 1297
 Perlmutter, S. et al., 1999, ApJ 517, 565
 Pope, A. C. et al., 2004, ApJ, 607, 655
 Riess A. G. et al., 1998, AJ 116, 1009

8 *Gaztañaga, Manera & Multamäki*

Sachs, R. K., Wolfe, A. M., 1967, ApJ 469, 437

Sandvik H.B., Tegmark M., Wang X., and Zaldarriaga M., Phys. Rev. D 69, 063005

Scranton, R. et al., 2003 astro-ph/0307335.

Tegmark, M. et al., 2004, ApJ, 606, 70